sustainability

MDPI

Article

Experimental Study on Adsorption Characteristics of Coal Gangue to Ca^{2+} in High-Salinity Mine Water

Nan Zhao [1], Ze Xia [1,*], Haokai Mu [2], Yukuan Fan [1] and Chuangkai Zheng [1]

[1] School of Mines, China University of Mining and Technology, Xuzhou 221116, China; 5126@cumt.edu.cn (N.Z.)
[2] China Construction Third Engineering Bureau Group South China Co., Ltd., Guangzhou 510540, China; ts22020163p21@cumt.edu.cn
* Correspondence: cumt_xiaze@cumt.edu.cn

Abstract

Targeting the purification of high-salinity mine water in ecologically vulnerable mining areas in Western China, this study conducted batch adsorption experiments using coal gangue from goaf areas to investigate the effects of initial Ca^{2+} concentration, treatment time, pH, temperature, and particle size on Ca^{2+} removal. The adsorption process was further elucidated through isotherm, kinetic, and thermodynamic modeling. The results demonstrate that the unique slit-shaped/plate-like mesoporous structure of coal gangue provides a favorable physical foundation for adsorption. Batch experiments identified optimal conditions at pH = 8 and 40 °C, achieving a maximum adsorption capacity of 12.4 mg/g. The process followed the Langmuir isotherm model (R^2 = 0.994, χ^2 = 0.122) and the pseudo-second-order kinetic model (R^2 = 0.952, χ^2 = 0.057), reaching equilibrium within 120 min. Thermodynamic analysis confirmed a spontaneous, endothermic, and entropy-driven process, with a relatively low heat of adsorption (ΔH < 20 kJ/mol) indicating physical adsorption as the dominant mechanism. Collectively, the adsorption system is characterized as a complex process governed by physical adsorption accompanied by weak chemical interactions and modulated by multiple environmental factors. Three mechanisms (electrostatic interaction, ion exchange, and surface complexation) jointly contribute to Ca^{2+} adsorption on coal gangue. This study enhances the understanding of the water purification mechanism by coal gangue, provides a theoretical basis for the application of underground coal mine reservoirs, and proposes a novel technical approach to mitigate membrane scaling caused by Ca^{2+} during mine water treatment.

Keywords: underground coal mine reservoir; high-salinity mine water; gangue pre-purification; adsorption characteristics

check for updates

Academic Editor: Agostina Chiavola

Received: 30 September 2025
Revised: 8 November 2025
Accepted: 17 November 2025
Published: 20 November 2025

Citation: Zhao, N.; Xia, Z.; Mu, H.; Fan, Y.; Zheng, C. Experimental Study on Adsorption Characteristics of Coal Gangue to Ca^{2+} in High-Salinity Mine Water. *Sustainability* **2025**, *17*, 10423. https://doi.org/10.3390/su172210423

Copyright: © 2025 by the authors. Licensee MDPI, Basel, Switzerland. This article is an open access article distributed under the terms and conditions of the Creative Commons Attribution (CC BY) license (https://creativecommons.org/licenses/by/4.0/).

1. Introduction

China's western mining regions (Shanxi, Shaanxi, Nei Mongol, Ningxia, and Xinjiang) are rich in coal resources and serve as key development bases for the country's coal resources. In 2023, the raw coal output of these western mining areas accounted for over 80% of the national total output [1]. However, coal mining operations require substantial water resources. The western mining areas are located in an arid zone with low precipitation, where the annual evaporation far exceeds the annual rainfall. These regions possess less than 10% of the nation's total water reserves yet account for approximately 16% of its water consumption [2]. Furthermore, the large-scale extraction of coal resources severely disrupts

the stable aquifer structures within the overlying strata. Strata movement alters the state of groundwater circulation, leading to environmental issues such as declining groundwater levels and water resource contamination [3–5]. The shortage of water resources is becoming increasingly critical in these ecologically vulnerable western regions. According to relevant statistics [6–8], the average water yield coefficient of coal mines in China is 1.87, with annual mine water inflow reaching as high as 668 million cubic meters. Nevertheless, the utilization rate of this water is only about 40%. Mine water in these ecologically vulnerable western regions is characterized by high salinity, typically presenting as neutral or weakly alkaline, with high total dissolved solids and elevated hardness [9,10]. Therefore, determining how to utilize mine water effectively is a crucial challenge for alleviating the coal-water conflict in these areas. Academician Gu [11,12] pioneered the theory and technological system of underground coal mine reservoirs, centered on "diversion, storage, and utilization," which has realized the resource utilization of mine water and been successfully implemented in the Shendong Mining Area. As research has progressed, subsequent studies have revealed that coal gangue in the goaf, rich in clay minerals with well-developed pore structures and favorable adsorption characteristics, can function as a natural purification medium within underground coal mine reservoirs, effectively improving mine water quality [6,8,13,14]. These findings provide theoretical support for the in situ purification and utilization of mine water.

Extensive studies have been conducted to examine the adsorption and purification mechanisms of coal gangue. Previous research has utilised various physicochemical characterization techniques [15–18] (including XRD, FTIR, SEM, Raman spectroscopy, BET, XPS, and zeta potential measurements) combined with adsorption isotherm, kinetic, and thermodynamic analyses to systematically reveal the intrinsic mechanisms of the adsorption process [19–21]. Building upon this foundation, Yao et al. [22] conducted dynamic adsorption experiments on coal gangue, investigating the isothermal adsorption characteristics of sandy mudstone for four types of heavy metal cations. Jiang et al. [23] experimentally found that coal gangue in the goaf can rapidly remove suspended solids from mine water and analyzed the purification mechanisms of underground coal mine reservoirs through simulation experiments. Guo et al. [24] utilized COMSOL numerical simulations to explore the dynamic adsorption characteristics of coal gangue under various influencing factors, revealing its adsorption mechanisms for heavy metal ions. Li et al. [25] designed dynamic leaching experiments and found that the adsorption capacity of gangue increases as its particle size decreases. Guo et al. [26] discovered that NaOH-modified coal gangue exhibits a relatively strong adsorption capacity for Fe^{2+} and Mn^{2+}. Li et al. [27] found that the adsorption characteristics of acid- and alkali-modified coal gangue for Pb^{2+} and Zn^{2+} both conform to the pseudo-second-order kinetic model. Zhao et al. [28] revealed that the abundant aluminosilicate minerals in coal gangue possess strong adsorption and degradation capabilities for organic matter in mine water. Proust et al. [29] found that clay minerals such as kaolinite and montmorillonite have excellent adsorption capacities for various heavy metal ions. The aforementioned research demonstrates that coal gangue in the goaf has a significant purifying effect on high-salinity mine water. These findings provide a new technical pathway for the treatment of high-salinity mine water underground.

Currently, commonly used methods for desalination of high-salinity mine water include chemical methods, membrane separation, and distillation. Among these, membrane-based desalination is widely employed in the concentration and desalination processes of high-salinity mine water [30–32]. However, its broad application is often constrained by membrane fouling caused by Ca^{2+} in high-salinity mine water, leading to substantially increased operational costs [10,33]. Although pretreatment processes such as chemical softening and ion exchange can partially mitigate this issue, these methods themselves face

challenges including high costs, potential secondary pollution, and process complexity. Therefore, developing an efficient, economical, and environmentally friendly pretreatment technology is crucial. The purification capability of underground coal mine reservoir technology offers a potential low-cost pretreatment solution, yet its specific removal mechanisms and efficacy for Ca^{2+} require further in-depth investigation. This study proposes that utilizing coal gangue, a solid waste from mining operations, as an adsorbent represents a promising strategy for achieving "waste–treats–waste" synergy. Combined with underground reservoir technology, this approach demonstrates significant potential for enhancing Ca^{2+} removal. However, current research on the adsorption performance of coal gangue has predominantly focused on heavy metal ions (such as Pb^{2+} and Cd^{2+}) or organic substances, while dedicated studies specifically targeting Ca^{2+} (a key scaling-prone ion) particularly regarding its adsorption mechanisms, migration and fixation processes, remain relatively limited.

Accordingly, coal gangue from a mining area in ecologically fragile mining areas of western China was selected as the research subject. Batch adsorption experiments were designed and conducted to systematically investigate the influence of various factors on Ca^{2+} adsorption behavior. Through integrated analysis of adsorption isotherms, kinetics, and thermodynamics, this work elucidates the "deprotonation-dominated surface complexation" mechanism for Ca^{2+} adsorption on coal gangue while providing an in-depth examination of Ca^{2+} migration and fixation processes within the gangue matrix. This will enrich our understanding of water purification mechanisms within underground coal mine reservoirs, while also proposing an efficient, economical pretreatment strategy for the membrane-based desalination of high-salinity mine water.

2. Materials and Methods

2.1. Adsorbent and Pretreatment

To ensure consistency in adsorbent source and subsequent experimental conditions, rock samples from the roof strata of the main mining seam in a coal mine located in ecologically fragile mining areas of western China were selected as the source of coal gangue for this study. The samples underwent preprocessing in the laboratory, including sampling, quartering, crushing, and sieving. Different particle size fractions were obtained for use in subsequent batch adsorption experiments, as illustrated in Figure 1.

After initial inspection and cleaning of the sample appearance, four sampling points were uniformly selected on the surface of the rock sample, and approximately 100 g of particulate matter was collected from each point and mixed. The combined sample was then further reduced by quartering and splitting to minimize sampling bias and improve representativeness. These steps ensured the uniformity and reproducibility of subsequent particle size preparation. To facilitate mechanical crushing, large pieces were first wiped on the surface and pre-crushed with a small hammer into smaller pieces suitable for machine input.

Prior to laboratory sampling, the samples underwent only surface cleaning without any further treatment, in order to preserve their natural state to the greatest extent possible. To maintain consistency with subsequent batch adsorption and isothermal experiments, four standard particle size ranges were adopted in this study: 10–20 mesh, 20–40 mesh, 40–60 mesh and 200 mesh. These were used as gradient levels of the "particle size" variable to compare the effects of specific surface area and external diffusion path on equilibrium adsorption.

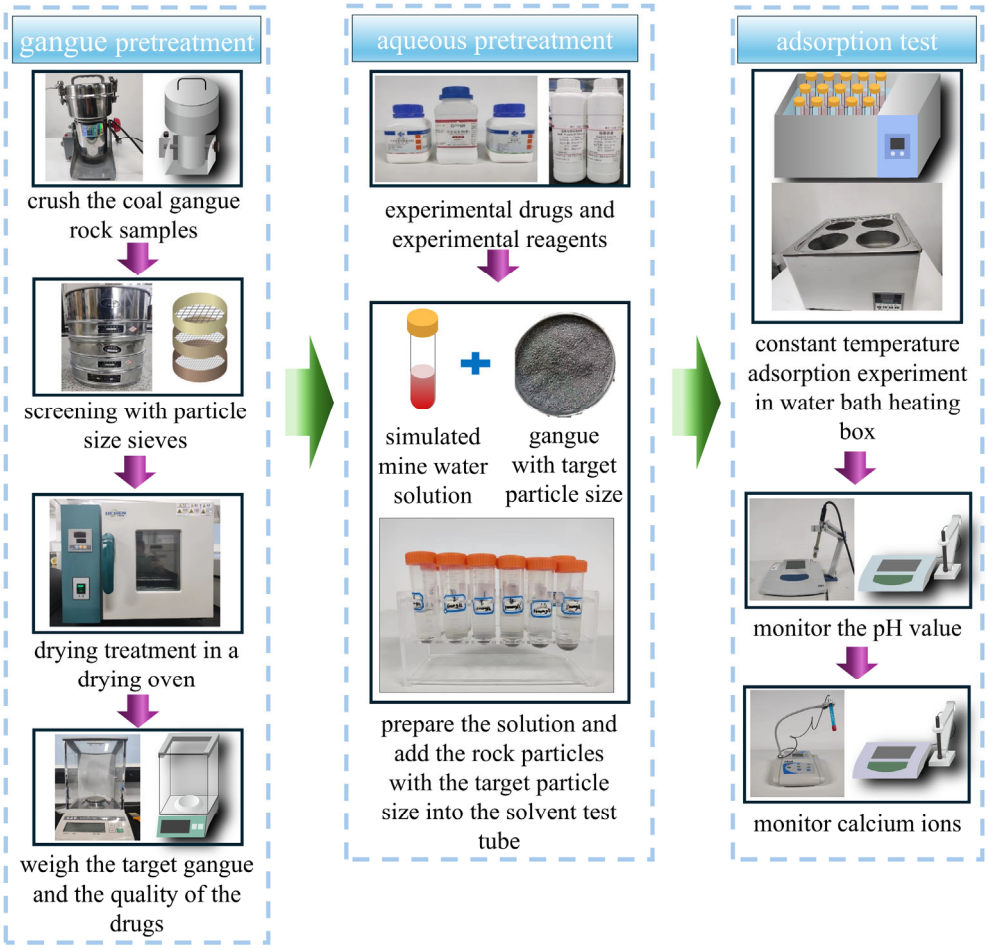

Figure 1. Experimental workflow and key apparatus for Ca^{2+} adsorption by coal gangue.

2.2. *Adsorbate and Solution Preparation*

The equipment used for preparing the experimental solutions primarily included a pH meter, pipette, measuring cylinder, and rubber-headed dropper. Solutions employed for pH adjustment consisted of 0.01002 mol/L HCl and 0.01002 mol/L NaOH. Deionized water was used throughout the experiments, and all chemical reagents selected had a purity greater than 99%. Table 1 lists the chemical substances and reagents employed during the experimental process.

Table 1. Main experimental Chemical drugs and reagents.

Chemical Reagents	Purity	Manufacturer
NaOH	0.01002 mol/L	Yida Technology Co., Ltd. Jurong, China
HCl	0.01002 mol/L	
$CaCl_2$	Analytical Reagent	Fuchen (Tianjin) Chemical Reagents Co., Ltd. Tianjin, China
$MgCl_2 \cdot 6H_2O$	Analytical Reagent	
KCl	Analytical Reagent	
Na_2SO_4	Analytical Reagent	
NaCl	Analytical Reagent	
$NaHCO_3$	Analytical Reagent	
H_2O	Analytical Reagent	

As indicated in Table 2, the predominant cations in the mine water of this coal mine are Ca^{2+}, Mg^{2+}, K^+ and Na^+, while the main anions consist of Cl^-, $SO_4{}^{2-}$ and $HCO_3{}^-$. The mine water exhibits weak alkalinity. A synthetic mine water solution was prepared based

on the measured ion concentrations of the actual mine water. To specifically investigate the influence of calcium ion concentration, the solution was initially formulated containing all ions except calcium. Calcium ions were added separately at a later stage according to the specific requirements of each experimental condition. The prepared solution is uniformly referred to as the "synthetic mine water solution" in the subsequent sections. The masses of chemicals required for the preparation of 1 L of this solution are listed in Table 3.

Table 2. The main ions in the mine water from sampling sites.

pH	Ion Concentration mg/L							TDS mg/L	Mineralization of Water mg/L	Water Hardness mg/L
	Ca^{2+}	Mg^{2+}	K^{+}	Na^{+}	Cl^{-}	$SO_4{}^{2-}$	$HCO_3{}^{-}$			
8.17	200.2	178.9	9.4	1378	1653.76	1292	488.74	4918.72	5163.08	1092.4

Table 3. Main pharmaceutical reagents.

Name	$MgCl_2{\cdot}6H_2O$	NaCl	KCl	$NaHCO_3$	Na_2SO_4
Mass/g	1.691	1.365	0.019	0.84	1.492

The preparation process for mine water solutions at different Ca^{2+} concentrations and pH values is as follows:

① First, all required equipment including beakers, measuring cylinders, and rubber-headed droppers were thoroughly cleaned with deionized water to ensure they were free of residual impurities. The cleaned glassware was then air-dried naturally until all moisture had completely evaporated before proceeding with solution preparation.

② Precisely measured quantities of $CaCl_2$ (0.2775 g, 0.41625 g, 0.555 g, 1.110 g, 1.665 g, 2.220 g, and 2.775 g) were weighed using a high-precision electronic balance (JJ224BC, G&G Measurement Plant, Changshu, China) and added to 1 L of the prepared mine water solution, followed by thorough stirring until complete dissolution was achieved.

③ Using a rubber-headed dropper, HCl solution was gradually added dropwise while simultaneously activating the stirring apparatus to ensure homogeneous mixing. The pH was monitored in real-time with a pH meter and finely adjusted until the solution reached pH 6. Subsequently, NaOH solution was slowly introduced via dropper while maintaining continuous stirring. Based on real-time pH readings, the solution was precisely adjusted to achieve target pH values of 8 and 9, respectively.

2.3. Characterization of Coal Gangue Materials

Mineral composition analysis was performed using an X-ray powder diffractometer (Figure 2a, Ultima IV, Rigaku Holdings Corporation, Tokyo, Japan) with a scanning range of 3° to 120° and a step size of 0.0001°. The measurements were conducted using Cu $K\alpha_1$ radiation (wavelength = 1.5406 A) generated at 3 kW. The silty mudstone samples were ground to 325-mesh powder, pressed into uniform thin sheets, and placed on the sample stage for XRD analysis. The crystal structure and properties were determined through interpretation of the diffraction patterns.

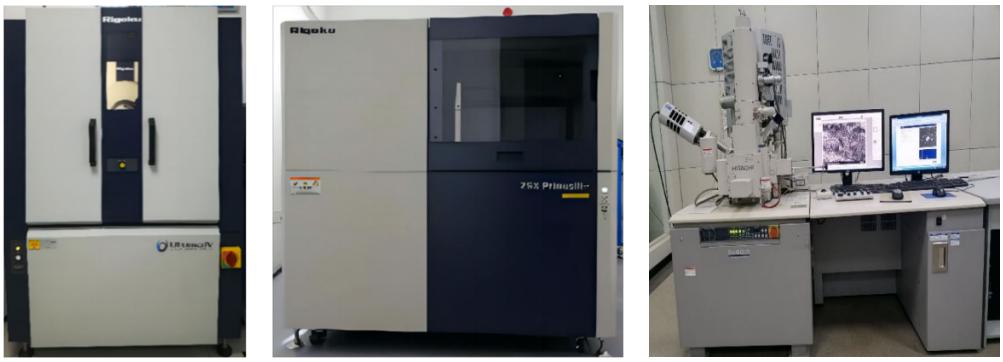

(**a**) (**b**) (**c**)

Figure 2. Main instruments for physicochemical characterization. (**a**) X-ray diffractometer; (**b**) X-ray fluorescence spectrometer; (**c**) scanning electron microscope.

Elemental quantitative analysis of the silty mudstone samples was carried out using a Rigaku X-ray fluorescence spectrometer (Figure 2b, ZSX Primus III+, Rigaku Holdings Corporation, Tokyo, Japan). The X-ray tube power was set at 4 kW, with analytical element coverage from ^{4}Be to ^{92}U. The scanning rate was 2400°/min, and the goniometer accuracy was ±0.0001°.

Specific surface area and pore structure were characterized by N2 adsorption–desorption isotherms using an ASAP 2460 extended automatic surface area and porosity analyzer (ASAP 2460, Micromeritics, Shanghai, China). The monolayer adsorption capacity of the samples was calculated according to Equation (1):

$$V = \frac{V_m pC}{(p_s - p)[1 - (p/p_s) + C(p/p_s)]} \times 100\% \quad (1)$$

where V represents the volume of adsorbed gas, m^3. V_m denotes the monolayer adsorption capacity, m^3. p indicates the equilibrium pressure of the adsorbed gas at the adsorption temperature, Pa. p_s is the saturation vapor pressure, Pa. C is a constant related to the heat of vaporization of the adsorbate.

Microstructural morphology of the silty mudstone was examined using a field emission scanning electron microscope (Figure 2c, SU5000, Hitachi, Beijing, China) under SEM operating conditions.

2.4. Batch Adsorption Experiment Design

Single-factor experiments were conducted to investigate the effects of pH, temperature, particle size, and initial calcium ion concentration on the adsorption of calcium ions onto coal gangue. The study aimed to characterize the isothermal adsorption behavior, adsorption kinetics, and adsorption thermodynamics of the rock particles. The specific design of the single-factor batch adsorption experiments is summarized in Table 4. For each experiment, only the factor under investigation was varied while keeping other conditions constant. Samples were collected at predetermined time intervals during the experiments. The Ca^{2+} concentration and pH of the supernatant were measured until the adsorption curve reached a plateau, indicating that equilibrium had been attained. The specific experimental steps are as follows:

① The initially crushed coal gangue was further processed using a mechanical crusher (Ronghao, Rh-600A, Yongkang Ronghao Industry & Trade Co., Ltd., Jinhua, China) and subsequently sieved through mesh screens of different apertures to obtain four particle size fractions: 10–20 mesh, 20–40 mesh, 40–60 mesh, and 200 mesh.

② The sieved rock particles were placed in an electric blast drying oven (Model LC-202/101, Lichen Scientific Instruments Co., Ltd., Shaoxing, China) and dried at 105 °C for 5 h.

③ Mine water solutions with different Ca^{2+} concentrations and pH values were prepared. Pre-weighed quantities of rock particles were measured using an electronic balance (Model JJ224BC, Shuangjie Testing Instrument Factory, Chuangshu, China) and placed in centrifuge tubes. The tubes were then positioned in a constant-temperature water bath (Model BSH, JoanLab Equipment (Zhejiang) Co., Ltd., Huzhou, China) to conduct batch adsorption experiments under various conditions.

④ A pH meter and a calcium ion-selective electrode (Model PXS-Ga, Hangzhou Qiwei Instrument Co., Ltd., Hangzhou, China) were employed to monitor changes in solution pH and Ca^{2+} concentration during the experiments. Intermittent sampling was conducted between 20 and 160 min to obtain concentration-time (C_t-t) and pH-time (pH-t) curves, monitoring both the initial rapid adsorption phase and the subsequent equilibrium phase.

Table 4. Single factor adsorption experiments.

Experiment Name	pH	Temperature (°C)	Ca^{2+} Concentration (mg/L)	Particle Size (Mesh)	Reaction Time (min)
Isothermal Adsorption	7	20	400, 600, 800, 1000	10–20	160
Adsorption Kinetics	7	20	1000	10–20	0–180
Adsorption Thermodynamics	7	10, 20, 30, 40	1000	10–20	0–160
Varying Initial Concentration	7	20	100, 150, 200, 400, 600, 800, 1000	10–20	0–210
Varying Reaction Time	7	20	400, 600, 800, 1000	10–20	0–160
Varying pH	6, 7, 8, 9	20	1000	10–20	160
Varying Temperature	7	20	1000	10–20	160
Varying Particle Size	7	20	1000	10–20, 20–40, 40–60, 200	210

The adsorption capacity (A), distribution coefficient (K_d), and removal efficiency (Y) were calculated according to the data analysis methods described in the respective section. The formulas used are as follows:

$$A = \frac{C_0 - C_e}{C_0} \times 100\% \quad (2)$$

$$K_d = \frac{(C_0 - C_e)V}{q_e m} \times 100\% \quad (3)$$

$$Y = \frac{W_1}{W} \quad (4)$$

where C_0 is the initial adsorbate concentration, mg/L. C_e is the equilibrium concentration, mg/L. q_e is the adsorption capacity per unit mass of adsorbent, mg/g. V is the total volume of the solution, L. m is the mass of the adsorbent, mg. W_1 and W refer to the amount of adsorbate adsorbed by the adsorbent and the total amount of adsorbate, respectively, mg.

3. Results

3.1. Key Characterization Results

Lithological identification results (Table 5) indicate that the silty mudstone is predominantly composed of sericite and silt-sized minerals, collectively accounting for over 90% of its constituents. Trace amounts of biotite, chlorite, other clay minerals, and opaque minerals are also present. The overall fabric of the rock exhibits a distinct preferred orientation.

Table 5. Characterization and identification of siltstone.

Rock Composition	Content	Characteristics
Sericite	≈62%	Fine flaky texture, grain size predominantly below 0.1 mm, formed by metamorphic crystallization of early mudstone. Colorless or slightly reddish-brown due to iron staining. Exhibits extremely perfect cleavage. Interference colors, primarily orange-yellow due to fine grain size, rarely reaching vivid secondary hues.
Silt-grade minerals	≈30%	Granular, typically less than 0.05 mm in size, showing weakly developed recrystallization. Mixed among clay and other components, primarily quartz silt grains with trace feldspar.
Biotite	<1%	Fine-scale flaky morphology, originating from early mud undergoing metamorphic crystallization. Size less than 0.05 mm, pale green or pale yellow-green in hue, with unusual interference colors.
Chlorite	≈3%	Often exhibits iron staining with a reddish-brown tint; shows weak optical properties under orthoptic polariscope.
Other clay minerals	≈3%	
Opaque minerals	≈1%	Commonly occurs as granular, plate-like, or lamellar textures; predominantly black or dark brown, likely dominated by iron-bearing minerals.
Rock structure		Granular-scaly metamorphic texture
Rock fabric		Plate-like foliation structure

X-ray fluorescence (XRF) analysis identifies the sample as a typical siliceous rock, characterized by a SiO_2 content exceeding 50%, an Al_2O_3 content over 20%, and an Fe_2O_3 content of approximately 7.004%, with MgO and K_2O contents ranging between 1–2% (Figure 3a). With a Al_2O_3/SiO_2 ratio of 0.47, the material is classified as having a medium Al_2O_3/SiO_2 ratio [34] and indicating a high abundance of clay minerals. This inference is confirmed by X-ray diffraction (XRD) analysis (Figure 3b), which reveals that the gangue's mineral composition is primarily composed of clay minerals (mainly chlorite and illite) and quartz. These clay minerals possess a substantial specific surface area and well-developed pore structures, properties that confer their exceptional adsorption capacity, efficient dehydration-rehydration characteristics, significant swelling-shrinkage behavior, and superior ion-exchange performance [35–38].

Figure 3c shows that the N_2 adsorption–desorption isotherm exhibits a type IV IUPAC classification with an H3-type hysteresis loop in the relative pressure range of $p/p^0 \approx 0.5$–1.0, indicating the predominance of slit-shaped/plate-like mesopores in the adsorbent structure [16]. As summarized in Table 6, the BET specific surface area, total pore volume, and average pore size of the silty mudstone are determined to be 10.1629 m^2/g, 0.0326 cm^3/g, and 6.4116 nm, respectively. A distinct capillary condensation inflection is observed at $p/p^0 \approx 0.5$, accompanied by a rapid increase in adsorption capacity, while the desorption curve lies above the adsorption curve, reflecting the confinement effect of pore geometry on the phase transition process. These pore structural characteristics align closely with the surface morphology revealed by multi-magnification SEM images

(Figure 3d), which display a complex structure comprising rough surfaces, flaky debris, and irregular pores/microfractures, indicating significant geometric heterogeneity and a potential "fissure-pore" interconnected network. The macro-morphology observed by SEM, described as "rough surface with developed intergranular pores and voids", corroborates the mesoporous structural features indicated by the H3 hysteresis loop. This unique structure combining surface roughness and mesoporous characteristics not only provides sufficient external surface exposure and effective diffusion pathways for Ca^{2+} but also offers robust morphological evidence for the enhanced equilibrium adsorption capacity observed under weakly alkaline conditions, achieved through improved external diffusion efficiency and diversified surface interaction modes.

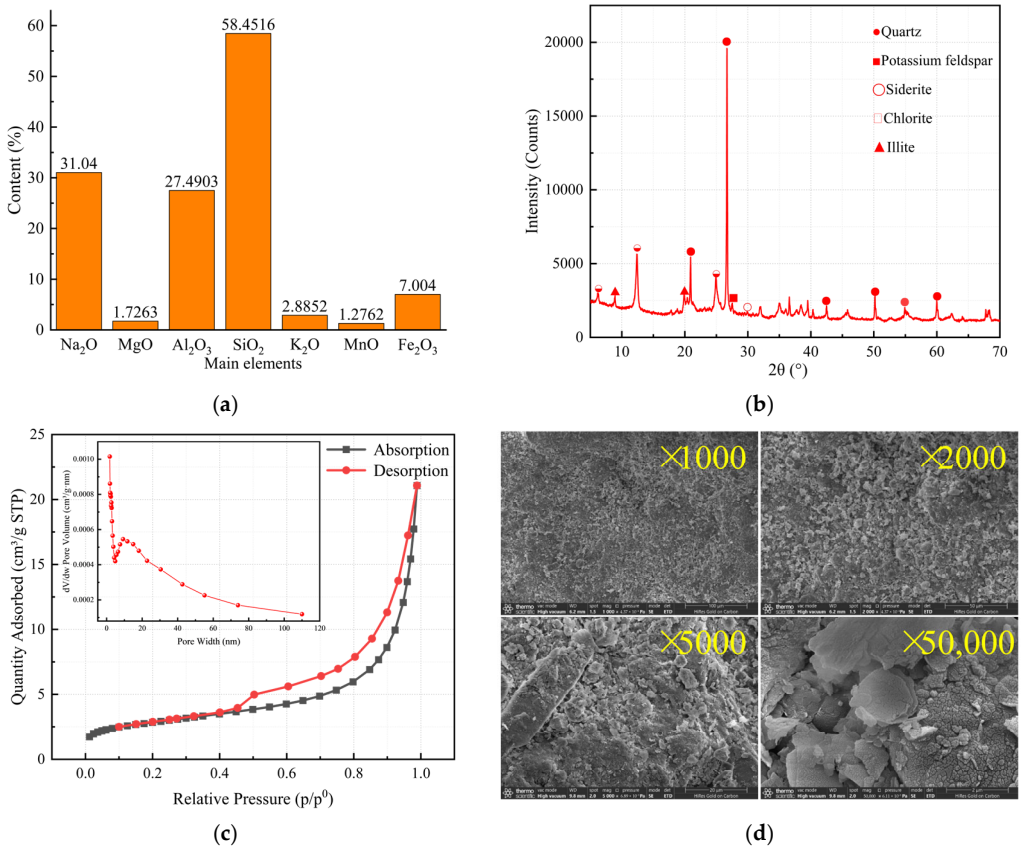

Figure 3. Test Results of Physical and Chemical Characteristics of Coal Gangue. (**a**) Column chart of main elements in coal gangue. (**b**) X-ray diffraction pattern. (**c**) N_2 adsorption–desorption curve of coal gangue. (**d**) SEM images of coal gangue at different.

Table 6. Surface area and pore characteristics.

Surface Area Results	Parameters
Total pore volume	0.0326 cm^3/g
Average pore size	6.4116 nm
BET surface area	10.1629 m^2/g

3.2. Analysis of Key Influencing Factors in the Adsorption Process

3.2.1. Effect of Initial Concentration and Reaction Time on Adsorption Performance

The influence of initial concentration and reaction time on the static removal of Ca^{2+} is summarized in Figure 4. Experiments were conducted with initial Ca^{2+} concentrations (C_0) of 400, 600, 800, and 1000 mg/L, during which samples were collected at intervals from

20 to 160 min for measurement of Ca^{2+} concentration (C_t) and pH. The results indicate that the C_t-t curves under different initial concentrations (C_0) consistently exhibited three distinct evolutionary stages: a rapid removal phase (0–40 min) characterized by a sharp decline in Ca^{2+} concentration, followed by a transition phase (40–100 min) with a noticeably reduced slope, and finally an equilibrium phase (after 100–120 min) where variations between consecutive samples were within experimental error. Based on these trends, the equilibrium time was established as 120 min and uniformly applied in subsequent static adsorption and isothermal modeling.

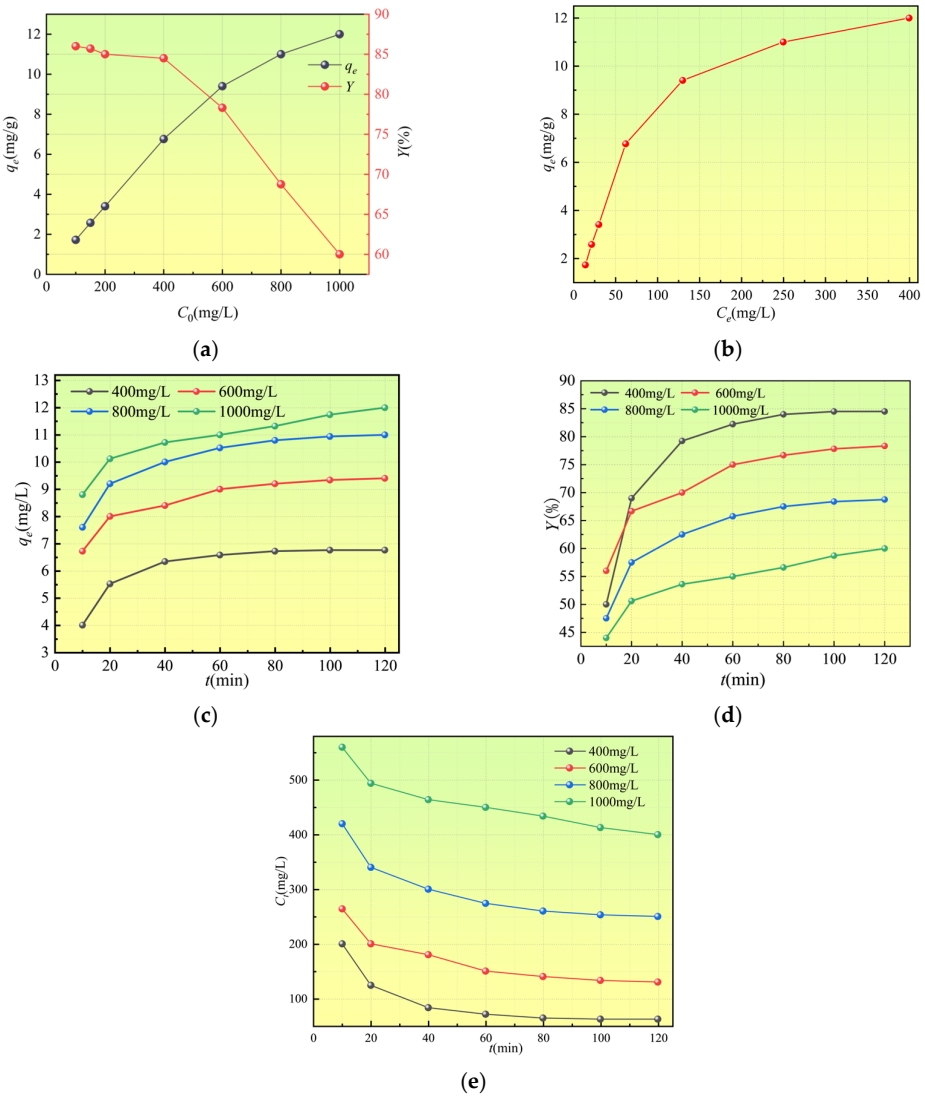

Figure 4. Influence of Initial Concentration and Reaction Time on the Static Removal of Ca^{2+}. (**a**) Variation in adsorption capacity and removal efficiency with concentration. (**b**) Relationship between equilibrium concentration and adsorption capacity. (**c**) Variation in adsorption capacity with time. (**d**) Variation in removal efficiency with time. (**e**) Variation of Ca^{2+} concentration with time.

The initial Ca^{2+} concentration exerted a pronounced influence on the adsorption equilibrium. As C_0 increased from 400 to 1000 mg/L, the equilibrium concentration (C_e) rose and the unit mass equilibrium adsorption capacity (q_e) increased synchronously, while the removal efficiency (Y) correspondingly declined. An initial Ca^{2+} concentration of approximately 600 mg/L was identified as the most favorable condition under the studied system.

3.2.2. Effect of pH on Adsorption Performance

Solution pH was identified as one of the predominant influencing factors for Ca^{2+} adsorption onto coal gangue. The effect of pH on adsorption efficiency is presented in Figure 5. Adsorption experiments conducted at different initial pH levels (6, 7, 8, and 9) revealed that the equilibrium adsorption capacity (q_e) initially increased with time before stabilizing, ultimately reaching adsorption equilibrium (Figure 5a). The Ca^{2+} adsorption performance (reflected by both q_e and removal efficiency Y) was significantly influenced by pH, showing synchronous enhancement as pH increased from 6 to 8, followed by a subsequent decline with further pH increase. This indicates that the surface chemistry of coal gangue is most favorable for Ca^{2+} adsorption under weakly alkaline conditions.

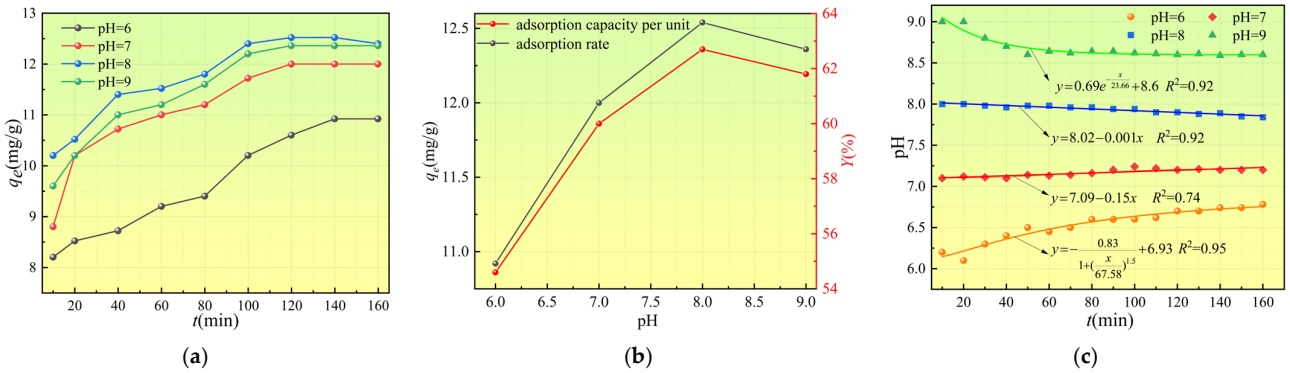

(**a**) (**b**) (**c**)

Figure 5. Effects of pH on Ca^{2+} adsorption by coal gangue. (**a**) Variation in adsorption capacity with pH. (**b**) Changes in adsorption capacity and removal efficiency under different equilibrium conditions. (**c**) pH evolution profile.

Further analysis suggests that under acidic conditions, the leaching of other metal cations from the coal gangue may compete with Ca^{2+} for adsorption sites, thereby inhibiting its removal. Possible reactions [8] occurring in the coal gangue-mine water system under such conditions are represented by Equations (5)–(9).

$$K_2O + 2H^+ = 2Na^+ + H_2O \quad (5)$$

$$Na_2O + 2H^+ = 2Na^+ + H_2O \quad (6)$$

$$CaO + 2H^+ = Ca^{2+} + H_2O \quad (7)$$

$$MgO + 2H^+ = Mg^{2+} + H_2O \quad (8)$$

$$H^+ + HCO_3^- = H_2O + CO_2 \quad (9)$$

Under alkaline conditions, OH^- promotes the formation of CO_3^{2-} in the solution, which subsequently combines with Ca^{2+} to form precipitates. This process acts synergistically with coal gangue adsorption, collectively enhancing the efficient removal of Ca^{2+}. Possible reactions [8] in the coal gangue-mine water system under alkaline conditions are illustrated by Equations (10) and (11).

$$HCO_3^- + OH^- = H_2O + CO_3^{2-} \quad (10)$$

$$Ca^{2+} + CO_3^{2-} = CaCO_3 \quad (11)$$

The adsorption performance of Ca^{2+} reached its optimum at pH = 8, while further increase in pH led to decreased adsorption efficiency (q_e and Y). As demonstrated in previous research [39], weakly alkaline conditions promote the formation of negatively

charged adsorption sites on the coal gangue surface, which significantly enhances the adsorption capacity of the adsorbent for the target substance.

The corresponding pH-*t* curves (Figure 5c) revealed a self-buffering characteristic of the system. All groups exhibited a certain degree of pH drift within the first 20–40 min, followed by stabilization. Specifically, systems starting under acidic conditions (pH = 6, 7) underwent significant upward adjustment, eventually stabilizing in the near-neutral to weakly alkaline range. In contrast, those beginning under weakly alkaline conditions (pH = 8, 9) showed only minor fluctuations before rapidly stabilizing. This behavior indicates that water-rock interactions and the buffering effect of the carbonate system collectively drive the system toward a weakly alkaline equilibrium. This regulatory trend correlates well with the higher q_e and Y observed under weakly alkaline conditions.

3.2.3. Effect of Temperature on Adsorption Performance

The experiments were conducted at reaction temperatures of T = 10, 20, 30, and 40 °C (Figure 6). The results demonstrate a clear monotonic enhancing effect of temperature on the static removal of Ca^{2+}: as T increased from 10 to 40 °C, C_t consistently decreased, while both q_e and Y increased synchronously, exhibiting a nearly linear or weakly curvilinear upward trend. Within the studied temperature range, the adsorption capacity q_e reached approximately 12.4 mg/g with a removal efficiency Y of about 62% at 40 °C, whereas both values were significantly lower at 10 °C. These findings indicate that the optimal temperature range for this system lies between 30 and 40 °C. Under unchanged other conditions, moderate heating within this range can yield stable and notable improvements in adsorption performance.

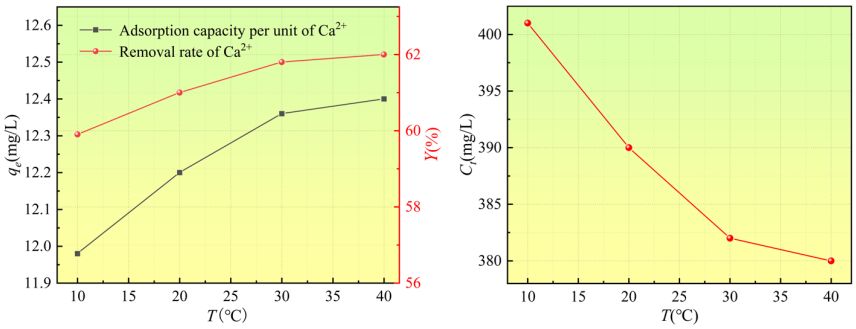

(**a**) (**b**)

Figure 6. Effect of Different Reaction Temperatures on Ca^{2+} Adsorption Performance. (**a**) Variation Curve of Adsorption Capacity. (**b**) Variation Curve of Equilibrium Concentration.

The enhancing effect of temperature on adsorption can be attributed to two synergistic mechanisms. Firstly, the increase in the diffusion coefficient of the solute and the mass transfer coefficient across the boundary layer with temperature facilitates the transport and occupancy of Ca^{2+} ions at surface adsorption sites; additionally, the slight shift of the carbonate equilibrium in the solution toward CO_3^{2-} may promote minor co-precipitation of $CaCO_3$ with Ca^{2+}, thereby working in concert with adsorption to reduce C_t. It should be emphasized, however, that in this system the precipitation pathway plays only a secondary role, while surface site occupation and ion exchange remain the dominant mechanisms.

3.2.4. Effect of Particle Size on Adsorption Performance

This study employed four particle size ranges (10–20, 20–40, 40–60, and 200 mesh) for comparative batch adsorption experiments (Figure 7). As shown in Figure 7, the equilibrium adsorption capacity (q_e) of coal gangue for Ca^{2+} exhibited a decreasing trend with increasing particle size. With the exception of the 200 mesh data points in the Langmuir

and Temkin models, the remaining data points were distributed below the fitted adsorption isotherm curves, though their overall distribution still followed the characteristic shape of typical adsorption isotherms. This observation indicates that particle size variation has limited influence on the adsorption performance of coal gangue, providing only marginal enhancement to the equilibrium adsorption capacity. Furthermore, the experimental baseline values for each particle size group remained consistent with those obtained in the single-factor experimental scheme.

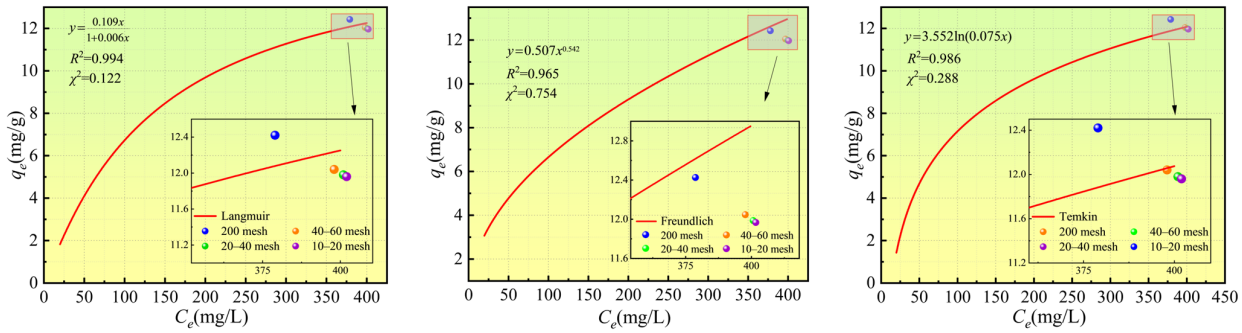

Figure 7. Effect of Particle Size on the Adsorption of Ca^{2+}. (**a**) Langmuir isothermal adsorption model. (**b**) Freundlich isothermal adsorption model. (**c**) Temkin isothermal adsorption model.

Previous studies have shown that, under constant adsorbent mass, reducing the particle size can effectively increase the specific surface area of the particles. This not only enhances the contact area between the particles and the surrounding environment but also increases the number of available adsorption sites. The greater availability of adsorption sites promotes interaction between the adsorbent and the target substance, thereby increasing the equilibrium adsorption capacity. The relatively minor effect observed in this study may be attributed to experimental error exceeding the actual influence of particle size, or to the fact that the selected size intervals were too narrow to produce significant differences in pore structure and adsorption behavior between adjacent fractions.

3.3. Isothermal Adsorption Characteristics of Ca^{2+}

Isothermal adsorption models were employed to analyze the adsorption mechanism of Ca^{2+} from high-salinity mine water onto coal gangue. The models applied include the Langmuir, Freundlich and Temkin isothermal adsorption models [40–44], expressed by Equation (12), Equation (13) and Equation (14), respectively.

$$q_e = \frac{q_{\max} b C_e}{1 + b C_e} \tag{12}$$

where C_e is the equilibrium concentration of the solution (mg/L), q_e is the adsorption capacity at equilibrium (mg/g), b is the adsorption constant, indicating the affinity between the adsorbent and adsorbate (L/mg), $q_{\max}$ is the maximum adsorption capacity of the adsorbent (mg/g).

$$q_e = K_f C_e^{1/n} \tag{13}$$

where K_f is the Freundlich adsorption constant, $1/n$ is the adsorption intensity parameter (adsorption is considered favorable when $1/n = 0.5$, adsorption becomes unfavorable when $1/n > 2$).

$$q_e = \frac{RT}{b_T} \ln(A_T C_e) \tag{14}$$

where T is the absolute temperature, K. R is the universal gas constant, 8.314 J/(mol K). A_T is the equilibrium binding constant corresponding to the maximum binding energy, L/g. b_T is Temkin isotherm constant, J/mol.

As shown in Figure 8, all three selected models demonstrate good fitting performance for the adsorption rate. To further evaluate the goodness-of-fit of different models, we calculated χ^2 as a statistical error metric and obtained fitting data for the Ca^{2+} adsorption isotherms (Table 7).

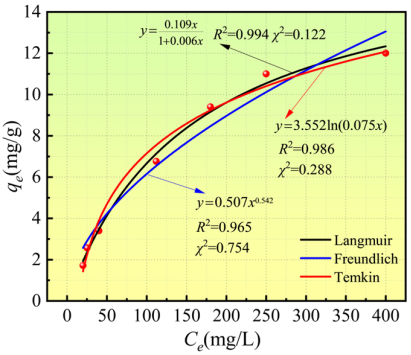

Figure 8. Isotherm adsorption fitting characteristic curve.

Table 7. Fitting data of Ca^{2+} adsorption isotherms.

Model	Fitting Parameters			
Langmuir	q_{max} (mg/L) 17.218	K_L (L/mg) 0.006	R^2 0.994	χ^2 0.122
Freundich	K_f 0.507	n 1.844	R^2 0.965	χ^2 0.754
Temkin	b_T (kJ/mol) 0.686	A_T (L/g) 0.075	R^2 0.986	χ^2 0.288

As presented in Table 5, during the removal of Ca^{2+} using coal gangue as the adsorbent medium, the Langmuir model (R^2 = 0.994, χ^2 = 0.122) achieved the highest prediction accuracy for the experimental data, suggesting that adsorption primarily occurs on relatively homogeneous sites and follows a monolayer adsorption mechanism. The Freundlich model fitting results (n = 1.844 > 1) indicate that the adsorption process of Ca^{2+} onto coal gangue is relatively favorable. Furthermore, the data reveal the coexistence of both monolayer and multilayer adsorption during the process, collectively influencing the adsorption behavior. The Temkin model (R^2 = 0.986, χ^2 = 0.2288) also exhibited high fitting accuracy, revealing a linear decrease in adsorption heat due to surface energy heterogeneity or intermolecular repulsion among adsorbates beneath the dominant monolayer adsorption. However, the obtained adsorption heat-related parameter is relatively small (b_T = 0.686 kJ/mol), indicating a gradual decline in adsorption heat with increasing coverage. This reflects the relatively uniform energy distribution on the coal gangue surface or weak lateral repulsion between adsorbed Ca^{2+} ions.

3.4. Adsorption Kinetics of Ca^{2+}

Adsorption kinetic models describe the rate processes of substance accumulation at interfaces. The pseudo-first-order kinetic model and pseudo-second-order kinetic model

are among the most widely used models for characterizing adsorption kinetics [45]. These models are mathematically represented by Equation (15) and Equation (16), respectively.

$$q_t = q_e\left(1 - e^{-k_1 t}\right) \tag{15}$$

where q_e is the adsorption capacity at equilibrium (mg/g), q_t is the adsorption capacity at time t (mg/g), k_1 is the pseudo-first-order rate constant (min^{-1}).

$$q_t = \frac{k_2 t {q_e}^2}{1 + k_2 t q_e} \tag{16}$$

where k_2 is the pseudo-second-order rate constant ($g \cdot mg^{-1} \cdot min^{-1}$), q_e is the maximum adsorption capacity (mg/g), q_t is the adsorption capacity at time t (mg/g).

The pseudo-first-order kinetic model is generally applicable to physical adsorption processes where the adsorption rate is proportional to the difference between the saturation capacity and the amount adsorbed at any time. It is commonly used to describe the initial stage of adsorption processes [46]. In contrast, the pseudo-second-order kinetic model is considered more suitable for describing the adsorption of heavy metal ions. This model assumes that the adsorption rate is determined by the chemical interaction between active sites on the adsorbent surface and metal ions, potentially involving electron transfer or sharing [47].

As summarized in Table 8, both the pseudo-first-order (R^2 = 0.952, χ^2 = 0.057) and pseudo-second-order (R^2 = 0.967, χ^2 = 0.039) models provide satisfactory fitting for the Ca^{2+} adsorption process. However, as shown in Figure 9, the pseudo-second-order model demonstrates superior agreement with experimental measurements. The higher R^2 value, lower χ^2 statistic, and closer match between the predicted (12.13 mg/g) and experimental (12.0 mg/g) equilibrium adsorption capacities collectively indicate that the pseudo-second-order model more accurately describes the Ca^{2+} adsorption process. Furthermore, the smaller fitting parameter k_2 obtained from the pseudo-second-order model suggests a gradual decrease in adsorption efficiency over time, which aligns with the previously observed decline in Ca^{2+} removal efficiency (Y) with prolonged reaction time. In conclusion, the adsorption process in this study is best described by the pseudo-second-order kinetic model and is primarily governed by chemical mechanisms.

Table 8. Ca^{2+} kinetic model adsorption data fitting.

Model	**Langmuir**				**Freundich**			
Parameters	q_e	k_1	R^2	χ^2	q_e	k_2	R^2	χ^2
	11.812	0.128	0.952	0.057	12.365	0.023	0.967	0.039

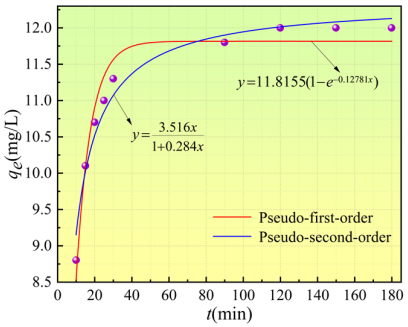

Figure 9. Ca^{2+} adsorption kinetic fitting curve.

3.5. Adsorption Thermodynamics

Adsorption thermodynamics investigates the thermodynamic properties and behavior of adsorbents during adsorption processes. Thermodynamic parameters provide critical insights into the spontaneity, feasibility, and mechanism of adsorption reactions. The extent and nature of adsorption can be interpreted through the values of ΔH, ΔS, and ΔG, whose relationships [48,49] are expressed by Equations (17) and (18). The thermodynamic fitting curves for Ca^{2+} adsorption onto coal gangue are presented in Figure 10, with corresponding parameters summarized in Table 9.

$$\ln K_d = -\frac{\Delta H}{R}\frac{1}{T} + \frac{\Delta S}{R} \tag{17}$$

$$\Delta G = \Delta H - T\Delta S \tag{18}$$

where ΔG represents Gibbs free energy, kJ/mol. ΔH denotes enthalpy change, kJ/mol. ΔS indicates entropy change, $kJ \cdot mol^{-1} \cdot K^{-1}$. K_d is the thermodynamic equilibrium constant for adsorption, representing the ratio of equilibrium adsorption amount to equilibrium concentration, and T is the absolute thermodynamic temperature, K. R is the gas constant, R = 8.314 $J \cdot mol^{-1} \cdot K^{-1}$.

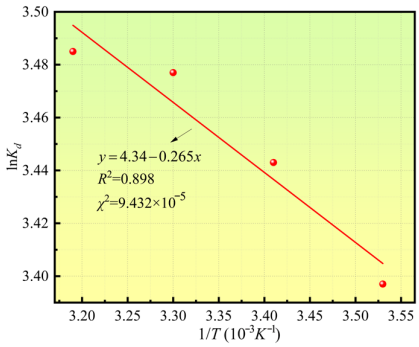

Figure 10. Ca^{2+} adsorption thermodynamic fitting curve.

Table 9. Ca^{2+} thermodynamic model adsorption data fitting.

Thermodynamic Parameters	*T*/K				R^2	χ^2
	281.5	291.5	300.5	315.5		
ΔH ($kJ \cdot mol^{-1}$)			2.203			
ΔS ($J \cdot mol^{-1} \cdot K^{-1}$)			36.084		0.898	9.432×10^{-5}
ΔG ($kJ \cdot mol^{-1}$)	−7.95	−8.31	−8.64	−9.18		

As shown in Figure 10 and Table 9, the positive ΔH values confirm the endothermic nature of the adsorption process, where elevated temperatures enhance adsorption capacity. The recorded ΔH values are all below 20 kJ/mol, indicating that physical adsorption dominates the mechanism [50]. The positive ΔS values suggest increased disorder of ions near the solid–liquid interface, resulting from accelerated ion transfer rates at higher temperatures. This phenomenon, known as the "entropy-driven" effect, reflects the increased entropy during adsorption. The negative ΔG values demonstrate spontaneous adsorption under the studied conditions, with more favorable adsorption occurring at higher temperatures.

4. Discussion

4.1. Synergistic Enhancement of Site Occupation-Dominated Adsorption by Weakly Alkaline Conditions and Moderate-to-High Temperatures

Under specified equilibrium time (120 min) and solid–liquid ratio conditions, this study reveals the crucial enhancement of Ca^{2+} adsorption performance by moderate-to-high Temperatures conditions and weakly alkaline environments. This synergistic mechanism can be interpreted from the following three perspectives:

(1) pH-Dependent Modulation of Surface Sites and the Deprotonation Effect

Adsorption experiments demonstrated that weakly alkaline conditions significantly enhanced Ca^{2+} adsorption onto coal gangue, as manifested by a decrease in the equilibrium concentration (C_e) and increases in both the equilibrium adsorption capacity (q_e) and removal efficiency (Y). This phenomenon can be attributed to changes in the surface chemistry of the coal gangue. Theoretically, under weakly alkaline conditions, hydroxyl functional groups such as Si-OH and Al-OH on the particle surface are more prone to deprotonation, forming negatively charged sites (e.g., Si-O^- and Al-O^-). These negatively charged sites not only strengthen the electrostatic attraction toward Ca^{2+} but also provide a more favorable interface for surface complexation.

The inference of improved site accessibility is supported by microstructural characterization: binarization-based quantitative analysis of SEM images (Figure 11) revealed increases in both porosity and pore number after treatment under weakly alkaline conditions, creating more favorable mass transfer conditions for adsorbate Ca^{2+} to access and occupy surface active sites. Ultimately, this adsorption behavior closely aligns with the Langmuir monolayer adsorption model, confirming a monolayer site occupation mechanism occurring on relatively homogeneous surfaces. The strong correlation among the observed pH effects, isotherm modeling, and microstructural changes forms a coherent evidence chain, robustly supporting the proposal that deprotonation-dominated surface complexation serves as the core adsorption mechanism.

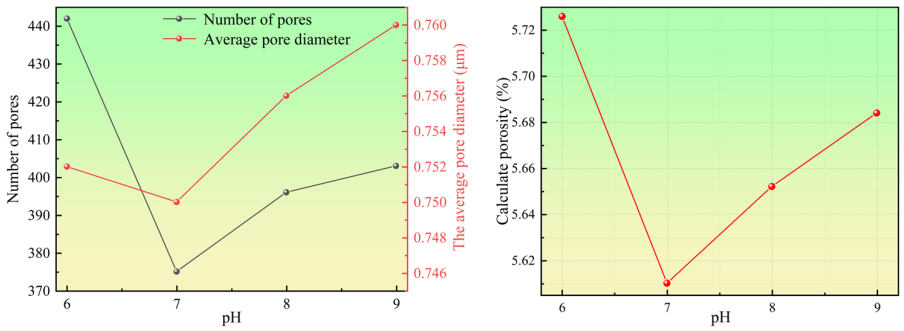

Figure 11. Variation in Surface Pore Parameters of Coal Gangue under Different pH Conditions. (**a**) Porosity under Different pH Conditions. (**b**) Pore Number and Average Pore Size under Different pH Conditions.

(2) Weak Synergistic Effect from the Solution Side

Under weakly alkaline conditions, the equilibrium between OH^- and HCO_3^- facilitates the formation of CO_3^{2-}, which can react with Ca^{2+} to form trace amounts of CaCO3. This precipitation pathway acts synergistically with surface site adsorption, collectively reducing the equilibrium Ca^{2+} concentration (C_e) in the solution. However, given the superior fitting of the Langmuir model and the relatively low heat of adsorption ($\Delta H < 20$ kJ/mol), it can be concluded that precipitation plays only a secondary role in this system, with physical adsorption remaining the dominant mechanism [44,51]. This also reasonably explains the

observed trend in adsorption efficiency with pH variation: performance was optimal at pH = 8, while further increasing to pH = 9 resulted in only marginal improvement. This diminished enhancement likely occurs because surface sites approach saturation at higher pH levels and increased negative surface charge may induce repulsive effects, thereby limiting additional gains in adsorption performance.

(3) Mass Transfer Promotion by Temperature and Thermodynamic Validation

Elevated temperature (10–40 °C) exhibited a clear monotonic enhancing effect on adsorption. From a kinetic perspective, the increase in temperature improved the diffusion coefficient of Ca^{2+} and the rate of ion transport across the boundary layer, enabling Ca^{2+} to reach and occupy surface active sites more rapidly. Thermodynamically, $\Delta H > 0$ indicates that the adsorption process is endothermic and thus favored at higher temperatures; $\Delta S > 0$ suggests a decrease in ordering at the interface and within the solvation layer, which facilitates and stabilizes monolayer occupation; and $\Delta G < 0$ confirms that the adsorption is spontaneous within the studied temperature range and becomes more favorable as temperature increases. These thermodynamic characteristics are consistent with a mixed mechanism dominated by physical adsorption accompanied by weak chemical interactions, aligning well with the monolayer site occupation mechanism described by the Langmuir model.

4.2. Establishment of the "Structure–Site–Performance" Relationship and the Weakened Particle Size Effect

Across the four investigated particle size fractions (from 10–20 mesh to 200 mesh), the reduction in particle size provided only limited enhancement to the equilibrium adsorption capacity (q_e). This phenomenon can be satisfactorily explained within the established closed-loop framework of the "structure–site–performance (Figure 12)" relationship.

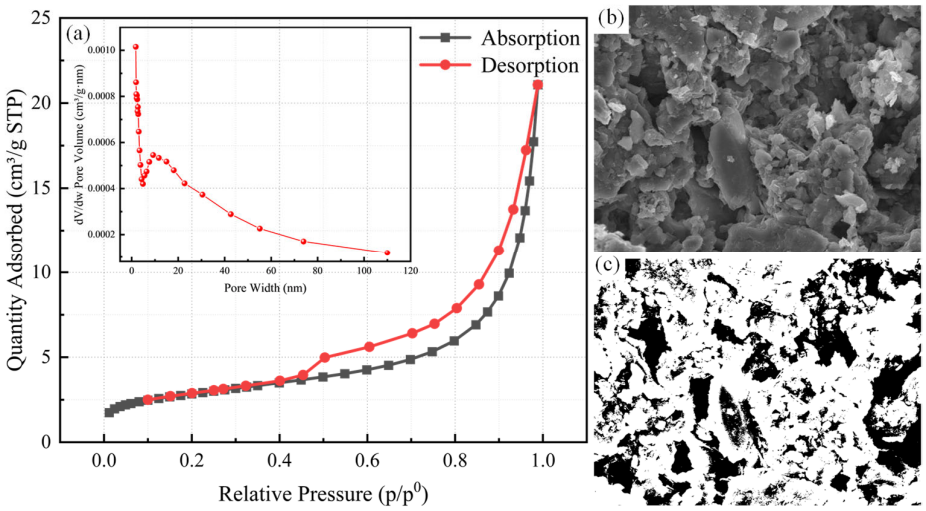

Figure 12. Evidence of the "Closed-Loop" Relationship Among Particle Size, Specific Surface Area, and Site Density. (**a**) N_2 adsorption–desorption curve of coal gangue. (**b**) Representative Raw SEM Image (pH = 8). (**c**) Binary-Processed SEM Field for Pore Counting.

(1) Abundant Accessible Sites Provided by the Intrinsic Porous Structure

As characterized in Section 3.1, the sample exhibits a mesopore-dominated type IV pore structure, a well-developed "fissure-pore" interconnected network, and a BET specific surface area of 10.1629 m^2/g. This implies that even for coarser particles, the external surface and internally connected channels already provide sufficient accessible surface area and abundant active sites for Ca^{2+}.

(2) Equilibrium Capacity Constrained by Total Site Density Rather Than Particle Size

High-precision fitting of the Langmuir model (R^2 = 0.994, χ^2 = 0.122) indicates that the adsorption equilibrium is ultimately determined by the total number of homogeneous monolayer sites (saturation capacity q_{max}) on the material surface. When these sites are substantially occupied within the unified equilibrium time of 120 min, further reducing the particle size to expose "new" sites yields diminishing marginal returns, as the total number of sites remains fundamentally unchanged.

(3) Adsorption Site Saturation Dominates Equilibrium Capacity

Although a reduction in particle size theoretically shortens the internal diffusion path and enhances the initial adsorption rate, all particle fractions approached or attained equilibrium within the 120-min treatment period. Therefore, the faster initial adsorption rates of finer particles did not yield a significant difference in the final equilibrium adsorption capacity.

In summary, this study elucidates that the adsorption of Ca^{2+} onto coal gangue is a complex process dominated by monolayer adsorption on an energetically heterogeneous surface. Based on comprehensive analysis of adsorption isotherms, kinetic characteristics, and material characterization results, it can be inferred that three mechanisms (electrostatic interaction, ion exchange, and surface complexation) collectively govern the adsorption effectiveness. Specifically, (1) electrostatic attraction is significantly enhanced under weakly alkaline conditions (pH $\approx$ 8) due to surface deprotonation, (2) the ion exchange process is supported by kinetic characteristics indicative of chemisorption, and (3) surface complexation stems from the coordination capability of hydroxyl sites in clay minerals under alkaline conditions. These three mechanisms operate synergistically at different stages or sites, collectively determining the final adsorption behavior and clearly delineating the intrinsic "structure–site–performance" relationship.

5. Conclusions

This study has systematically investigated the effects of initial Ca^{2+} concentration, reaction time, pH, temperature, and particle size on the removal of Ca^{2+} from high-salinity mine water by coal gangue through batch adsorption experiments. The research was complemented by analysis of adsorption isotherm characteristics, adsorption kinetics, and adsorption thermodynamics. The main findings are summarized as follows:

The adsorption of Ca^{2+} onto coal gangue represents a complex process, predominantly governed by physical adsorption accompanied by weak chemical interactions, and regulated by multiple environmental factors. Under weakly alkaline (pH = 8) and moderate-to-high temperature (40 °C) conditions, the adsorption performance reached its optimum, with an equilibrium adsorption capacity of approximately 12.4 mg/g. These conditions effectively promote the deprotonation of hydroxyl functional groups on the coal gangue surface, enhancing its electrostatic attraction and complexation capability toward Ca^{2+}, while trace co-precipitation in the solution exerts a positive synergistic effect.

The adsorption kinetic behavior was best described by the pseudo-second-order kinetic model (R^2 = 0.967, χ^2 = 0.039), suggesting that the rate-controlling step is governed by surface chemical interactions, potentially involving electron sharing or ion exchange. The adsorption process reached equilibrium within approximately 120 min, exhibiting a characteristic three-stage pattern of "rapid–transition–equilibrium".

Thermodynamic analysis confirmed the adsorption to be a spontaneous ($\Delta G < 0$), endothermic ($\Delta H > 0$), and entropy-driven ($\Delta S > 0$) process. These results provide a thermodynamic explanation for the enhanced adsorption at elevated temperatures and

are consistent with the conclusions from the kinetic studies, collectively revealing the fundamental nature of the adsorption mechanism.

The Langmuir isotherm model demonstrated the best goodness-of-fit to the experimental data (R^2 = 0.994, χ^2 = 0.122), indicating that adsorption primarily occurs on surface sites with a relatively uniform energy distribution and follows a monolayer mechanism. The well-developed mesoporous structure and rough surface of the coal gangue provide abundant accessible sites, which explains why variations in particle size within the tested range had only a limited effect on the equilibrium adsorption capacity.

These findings provide valuable insights into the mechanisms of coal gangue as an adsorbent for purifying high-salinity mine water and offer theoretical support for its in situ treatment applications. Additionally, the study presents an efficient and economical pretreatment approach for membrane-based desalination processes, showing potential to alleviate membrane fouling and reduce overall operational costs. However, constrained by experimental conditions, this study did not comprehensively address the effect of particle size on adsorption performance, nor did it thoroughly investigate the competitive adsorption behavior in multi-ion systems simulating real mine water. Future work will focus on these two aspects to further elucidate the adsorption characteristics and mechanisms of coal gangue in complex aqueous environments.

Author Contributions: N.Z.: Conceptualization, Methodology, Writing—original draft, formal analysis; Z.X.: Methodology, writing—review and editing; H.M.: investigation, data curation, conceptualization; Y.F.: visualization, conceptualization; C.Z.: data curation, conceptualization. All authors have read and agreed to the published version of the manuscript.

Funding: This research received no external funding.

Data Availability Statement: The original contributions presented in this study are included in the article. Further inquiries can be directed to the corresponding author.

Acknowledgments: The author gratefully acknowledge all the professors for their guidance and help during testing and writing.

Conflicts of Interest: Co-author Mu Haokai is currently employed by China Construction Third Engineering Bureau Group South China Co., Ltd. The remaining authors declare that this research did not involve any commercial or financial relationships that could constitute a potential conflict of interest.

References

1. Li, Y.H.; Yao, Q.L.; Xia, Z.; Yu, L.; Liu, Z.; Chen, S. Stability Evaluation of the Artificial Dam in Underground Reservoirs Under Storage and Drainage Cycles: A Method Based on Concrete Performance and Case Study. *Rock Mech. Rock Eng.* **2025**, *58*, 7725–7744. [CrossRef]
2. Yao, Q.L.; Yu, L.Q.; Chen, S.Y.; Li, Y.H.; Li, X.H. Mining-affected water resources and ecological effects in ecologically fragile mining areas of western China. *J. China Coal Soc.* **2025**, *50*, 748–767. [CrossRef]
3. Yao, Q.L.; Tang, C.J.; Liu, Z.C. Analysis of coal and water co-mining in ecologically fragile mining areas in Western China. *Coal Sci. Technol.* **2021**, *49*, 225–232. [CrossRef]
4. Wang, W.N.; Yao, Q.L.; Xu, Q.; Chen, X.Y.; Liu, H.Y.; Li, X.H. Experimental Study on the Evolution Law of Coal Mine Underground Reservoir Water Storage Space under the Disturbance and Water-Rock Interaction Effect. *Minerals* **2022**, *12*, 1491. [CrossRef]
5. Xu, Q.; Yao, Q.L.; Wang, F.R.; Xiao, L.; Ma, J.Q.; Kong, F.L.; Shang, X.B. Tracer Test Method to Confirm Hydraulic Connectivity Between Goafs in a Coal Mine. *Mine Water Environ.* **2024**, *43*, 104–116. [CrossRef]
6. Yao, Q.L.; Huang, G.; Xu, Q.; Zhu, L.; Guo, H.T. Experimental study on pre-treatment of high-mineralization mine drainage using gangue of different particle sizes. *J. Green Mine* **2024**, *2*, 122–129. [CrossRef]
7. Gu, D.Z.; Li, J.F.; Cao, Z.G.; Wu, B.Y.; Jiang, B.B.; Yan, Y.; Yan, J.; Chen, Y.P. Technology and engineering development strategy of water protection and utilization of coal mine in China. *J. China Coal Soc.* **2021**, *46*, 3079–3089. [CrossRef]
8. Zhu, L.; Yao, Q.L.; Xu, Q.; Li, Y.H.; Li, X.H. Experimental Study on the Purification Mechanism of Mine Water by Coal Gangue. *Water* **2023**, *15*, 697. [CrossRef]

9. Sun, Y.J.; Chen, G.; Xu, Z.M.; Yuan, H.Q.; Zhang, Y.Z.; Zhou, L.J.; Wang, X.; Zhang, C.H.; Zhang, J.M. Research progress of water environment, treatment and utilization in coal mining areas of China. *J. China Coal Soc.* **2020**, *45*, 304–316. [CrossRef]
10. Hu, X.; Zhang, Q. Mine Water Treatment, Resource Utilization and Prospects in Coal Mining Areas of Western China. *Mine Water Environ.* **2024**, *43*, 210–230. [CrossRef]
11. Gu, D.Z.; Cao, Z.G.; Li, J.F.; Wu, B.Y.; Zhang, Y.; Jiang, B.B.; Guo, Q.; Wang, H.P.; Wu, Y.; Shi, X.M.; et al. Original experimental platform system and application of under-ground coal mine reservoirs. *J. China Coal Soc.* **2024**, *49*, 100–113. [CrossRef]
12. Gu, D.Z. Theory framework and technological system of coal mine underground reservoir. *J. China Coal Soc.* **2015**, *40*, 239–246. [CrossRef]
13. Yao, Q.L.; Wang, W.N.; Xia, Z.; Zhu, L.; Wang, A.; Yu, L.Q. Adsorption characteristics of Mn (II) on sandy mudstone and fine sand-stone of coal measures. *J. China Univ. Min. Technol.* **2020**, *49*, 411–418. [CrossRef]
14. Wang, F.T.; Sun, N.; Zhang, C.; Fan, C.H.; Xiong, J.B.; Wei, X.Q.; Hao, W.H. Experimental study on mine water purification mechanism for broken coal and rock masses in the underground reservoir of ecologically vulnerable mining area. *Environ. Sci. Pollut. Res.* **2024**, *31*, 21442–21457. [CrossRef]
15. Gnanamoorthy, G.; Yadav, V.K.; Yadav, K.K.; Ramar, K.; Alam, J.; Shukla, A.K.; Ali, F.A.A.; Alhoshan, A. Fabrication of different SnO_2 nanorods for enhanced photocatalytic degradation and antibacterial activity. *Environ. Sci. Pollut. Res.* **2023**, *30*, 71574–71584. [CrossRef]
16. Shukla, A.K.; Alam, J.; Alhoshan, M. Trimesoyl chloride crosslinked chitosan: An efficient adsorbent for Congo red dye removal from water—Kinetic and isotherm analysis. *Int. J. Biol. Macromol.* **2025**, *319*, 145538. [CrossRef] [PubMed]
17. Rajabathar, J.R.; Shukla, A.K.; Ali, A.; Al-Lohedan, H.A. Silver nanoparticle/r-graphene oxide deposited mesoporous-manganese oxide nanocomposite for pollutant removal and supercapacitor applications. *Int. J. Hydrogen Energy* **2017**, *42*, 15679–15688. [CrossRef]
18. Shukla, A.K.; Alam, J.; Mallik, S.; Ruokolainen, J.; Kesari, K.K.; Alhoshan, M. Optimization and prediction of dye adsorption utilising cross-linked chitosan-activated charcoal: Response Surface Methodology and machine learning. *J. Mol. Liq.* **2024**, *411*, 125745. [CrossRef]
19. Mahdi, A.E.; Ali, N.S.; Majdi, H.S.; Albayati, T.M.; Abdulrahman, M.A.; Jasim, D.J.; Kalash, K.R.; Salih, I.K. Effective adsorption of 2-nitroaniline from wastewater applying mesoporous material MCM-48: Equilibrium, isotherm, and mechanism investigation. *Desalination Water Treat.* **2023**, *300*, 120–129. [CrossRef]
20. Al-Hazmi, G.A.A.M.; Alayyafi, A.A.; El-Desouky, M.G.; El-Bindary, A.A. Guava seed activated carbon loaded calcium alginate aerogel for the adsorption of diclofenac sodium: Characterization, isotherm, kinetics, and optimization via Box-Behnken design. *Int. J. Biol. Macromol.* **2024**, *262*, 129995. [CrossRef]
21. Alotaibi, A.M.; Alnawmasi, J.S.; Alshammari, N.A.H.; Abomuti, M.A.; Elsayed, N.H.; El-Desouky, M.G. Industrial dye absorption and elimination from aqueous solutions through bio-composite construction of an organic framework encased in food-grade algae and alginate: Adsorption isotherm, kinetics, thermodynamics, and optimization by Box–Behnken design. *Int. J. Biol. Macromol.* **2024**, *274*, 133442. [CrossRef]
22. Yao, Q.L.; Xia, Z.; Tang, C.J.; Zhu, L.; Wang, W.N.; Chen, T.; Tan, Y.M. Characteristics of Heavy Metal Ion Adsorption by Silty Mudstones in Coal Mine Goafs. *Geofluids* **2020**, *2020*, 8560151. [CrossRef]
23. Jiang, B.B.; Li, J.F.; Ma, L.Q.; Wu, M.; Su, C.; Li, J.H. Investigation of the suspended solids removal from mine water by the rock accumulation effect in the underground reservoir of coal mines. *Coal Sci. Technol.* **2024**, *52*, 352–361. [CrossRef]
24. Guo, Y.C.; Huang, Y.L.; Li, J.M.; Ouyang, S.Y.; Fan, B.T.; Liu, Y.H. Study on dynamic adsorption characteristics of gangue to heavy metals in goaf and its water purification mechanism under leaching condition. *J. Water Process Eng.* **2023**, *53*, 103741. [CrossRef]
25. Li, J.M.; Huang, Y.L.; Li, W.; Guo, Y.C.; Ouyang, S.Y.; Cao, G.L. Study on dynamic adsorption characteristics of broken coal gangue to heavy metal ions under leaching condition and its cleaner mechanism to mine water. *J. Clean. Prod.* **2021**, *329*, 129756. [CrossRef]
26. Guo, X.Y.; Dong, Y.R.; Di, J.Z.; Li, Y. Modified Gangue for Coal Mine Wastewater's Fe^{2+} and Mn^{2+} Adsorption. *Non-Met. Mines* **2017**, *40*, 83–87.
27. Liu, B.Y.; Li, S.W.; Song, Y.H.; Yao, Y.X.; Zhou, J.J.; Guo, C.B. Adsorption performance of modified coal gangue for Pb^{2+} and Zn^{2+} in wastewater. *J. Liaoning Tech. Univ. (Nat. Sci.)* **2023**, *42*, 444–450. [CrossRef]
28. Zhao, L.; Sun, Y.F.; Yang, B.B.; Wang, S.D.; Yang, J.; Sun, C.; Tian, Y.F. Removal efficiencies of dissolved organic matter and ammonium in coalmine water by coal gangue through column experiments. *J. China Coal Soc.* **2018**, *43*, 236–241. [CrossRef]
29. Proust, D. Sorption and distribution of Zn in a sludge-amended soil: Influence of the soil clay mineralogy. *J. Soils Sediments* **2015**, *15*, 607–622. [CrossRef]
30. Wang, X.F.; Gao, Y.B.; Jiang, X.J.; Zhang, Q.; Liu, W.G. Analysis on the Characteristics of Water Pollution Caused by Underground Mining and Research Progress of Treatment Technology. *Adv. Civ. Eng.* **2021**, *2021*, 9984147. [CrossRef]
31. Shah, K.M.; Billinge, I.H.; Chen, X.; Fan, H.; Huang, Y.; Winton, R.K.; Yip, N.Y. Drivers, challenges, and emerging technologies for desalination of high-salinity brines: A critical review. *Desalination* **2022**, *538*, 115827. [CrossRef]

32. Wang, C.S.; Liu, L.; Wang, Y.X.; Hou, P.; Wang, J.B.; Wang, J.W. Treatment of various saline wastewaters by membrane distillation with omniphobic polyvinyl alcohol membrane. *Desalination* **2024**, *591*, 118011. [CrossRef]
33. Ruiz, S.G.; López-Ramírez, J.A.; Zerrouk, M.H.; Lopera, A.E.C.; Alonso, J.M.Q. Study of reverse osmosis membranes fouling by inorganic salts and colloidal particles during seawater desalination. *Chin. J. Chem. Eng.* **2020**, *28*, 733–742. [CrossRef]
34. *GB/T 29162-2012*; General Administration of Quality Supervision, Inspection and Quarantine of the People's Republic of China, & Standardization Administration of the People's Republic of China. Classification of Gangue. China Standards Press: Beijing, China, 2013.
35. Zhao, S.S.; Chen, K.; Xiong, B.L.; Guo, C.L.; Dang, Z. Prediction of adsorption of metal cations by clay minerals using machine learning. *Sci. Total Environ.* **2024**, *924*, 171733. [CrossRef] [PubMed]
36. Zhu, R.L.; Chen, Q.Z.; Zhou, Q.; Xi, Y.F.; Zhu, J.X.; He, H.P. Adsorbents based on montmorillonite for contaminant removal from water: A review. *Appl. Clay Sci.* **2016**, *123*, 239–258. [CrossRef]
37. Chen, C.; Liu, H.B.; Chen, T.H.; Chen, D.; Frost, R.L. An insight into the removal of Pb(II), Cu(II), Co(II), Cd(II), Zn(II), Ag(I), Hg(I), Cr(VI) by Na(I)-montmorillonite and Ca(II)-montmorillonite. *Appl. Clay Sci.* **2015**, *118*, 239–247. [CrossRef]
38. Yao, S.; Feng, G.R.; Zhao, D.K.; Liu, A.F.; Du, J.; Wang, S.; Yao, X.; Hou, K. Research Progress of Clay Minerals in the Field of Coal Mine Water Treatment. *Mater. Rep.* **2025**, *39*, 71–80. Available online: https://link.cnki.net/urlid/50.1078.tb.20241206.0905.002 (accessed on 29 October 2025).
39. Gan, W.B.; Liu, Q. Coagulation of bitumen with kaolinite in aqueous solutions containing Ca^{2+}, Mg^{2+} and Fe^{3+}: Effect of citric acid. *J. Colloid Interface Sci.* **2008**, *324*, 85–91. [CrossRef]
40. Tenea, A.G.; Dinu, C.; Rus, P.A.; Ionescu, I.A.; Gheorghe, S.; Iancu, V.I.; Vasile, G.G.; Pascu, F.L.; Chiriac, F.L. Exploring adsorption dynamics of heavy metals onto varied commercial microplastic substrates: Isothermal models and kinetics analysis. *Heliyon* **2024**, *10*, e35364. [CrossRef]
41. Wu, J.; Wang, Q.; Wu, W.; Khor, S.M. Absorbent cotton-templated manganese oxide nanocomposites for methylene blue promote isothermal adsorption. *Int. J. Environ. Sci. Technol.* **2024**, *21*, 417–430. [CrossRef]
42. Simić, M.; Petrović, J.; Koprivica, M.; Ercegović, M.; Dimitrijević, J.; Vuković, N.S.; Fiol, N. Efficient Adsorption of Lead on Hydro-Pyrochar Synthesized by Two-Step Conversion of Corn Cob in Magnesium Chloride Medium. *Toxics* **2025**, *13*, 459. [CrossRef]
43. Alsuhaibani, A.M.; Alayyafi, A.A.; Albedair, L.A.; El-Desouky, M.G.; El-Bindary, A.A. Efficient fabrication of a composite sponge for Cr(VI) removal via citric acid cross-linking of metal-organic framework and chitosan: Adsorption isotherm, kinetic studies, and optimization using Box-Behnken design. *Mater. Today Sustain.* **2024**, *26*, 100732. [CrossRef]
44. Deng, J.H.; Ma, Z.T.; Qin, Q.Z.; Liu, W.L.; Wang, B. A residue reutilization strategy on fluorine-containing water purification. *J. Clean. Prod.* **2022**, *371*, 133613. [CrossRef]
45. Wang, J.L.; Guo, X. Adsorption kinetics and isotherm models of heavy metals by various adsorbents: An overview. *Crit. Rev. Environ. Sci. Technol.* **2023**, *53*, 1837–1865. [CrossRef]
46. Alshammari, N.A.H.; Alnawmasi, J.S.; Alotaibi, A.M.; Alshammari, O.A.O.; Abomuti, M.A.; Elsayed, N.H.; El-Bindary, A.A. Efficient adsorption of fluorescein dye from aqueous solutions by Al/Th-MOF bimetal-organic frameworks: Adsorption isotherm, kinetics, DFT computation, and optimization via Box-Behnken design. *Process Saf. Environ. Prot.* **2024**, *190*, 353–371. [CrossRef]
47. Wang, W.J.; Lin, J.X.; Shao, S.B.; Chen, H.J.; Dai, J.W.; Yang, Y. Enhanced adsorption of benzo(a)pyrene in soil by porous biochar: Adsorption kinetics, thermodynamics, and mechanisms. *J. Environ. Chem. Eng.* **2023**, *11*, 109002. [CrossRef]
48. Masuku, M.; Nure, J.F.; Atagana, H.I.; Hlongwa, N.; Nkambule, T.T.I. Pinecone biochar for the Adsorption of chromium (VI) from wastewater: Kinetics, thermodynamics, and adsorbent regeneration. *Environ. Res.* **2024**, *258*, 119423. [CrossRef] [PubMed]
49. Zhu, H.L.; Chen, S.N.; Duan, H.Y.; He, J.; Luo, Y.C. Removal of anionic and cationic dyes using porous chitosan/carboxymethyl cellulose-PEG hydrogels: Optimization, adsorption kinetics, isotherm and thermodynamics studies. *Int. J. Biol. Macromol.* **2023**, *231*, 123213. [CrossRef]
50. Yang, S.C.; Wang, P.; Wang, W.C.; Cao, Z.; Cao, Y.D. Study on the variability of oxygen adsorption behavior in coal gangue based on pore size structure. *Mater. Today Commun.* **2024**, *41*, 110657. [CrossRef]
51. Al-Hazmi, G.H.; Albedair, L.A.; Alatawi, R.A.S.; Alnawmasi, J.S.; Alsuhaibani, A.M.; El-Desouky, M.G. Enhancing trimethoprim pollutant removal from wastewater using magnetic metal-organic framework encapsulated with poly (itaconic acid)-grafted crosslinked chitosan composite sponge: Optimization through Box-Behnken design and thermodynamics of adsorption parameters. *Int. J. Biol. Macromol.* **2024**, *268*, 131947. [CrossRef]

Disclaimer/Publisher's Note: The statements, opinions and data contained in all publications are solely those of the individual author(s) and contributor(s) and not of MDPI and/or the editor(s). MDPI and/or the editor(s) disclaim responsibility for any injury to people or property resulting from any ideas, methods, instructions or products referred to in the content.